Dielectric relaxation and phase transition behavior of (1-*x*)$Pb(Zn_{1/3}Nb_{2/3})O_3$-*x*$BaTiO_3$ binary solid solutions

Qiang Gao, Qingyuan Hu, Li Jin, M.V. Gorev, D.S. Chezganov, E.O. Vlasov, Huarong Zeng, Luyang Zhao, Yu Cui, Zhuo Xu, Xiaoyong Wei

[a]*Electronic Materials Research Laboratory, Key Laboratory of the Ministry of Education & International Center for Dielectric Research, Xi'an Jiaotong University, Xi'an 710049, China*

[b]*Kirensky Institute of Physics, Federal Research Center KSC SB RAS, Krasnoyarsk 660036, Russia*

[c]*Institute of Engineering Physics and Radio Electronics, Siberian Federal University, Krasnoyarsk, 660041, Russia*

[d]*State Key Laboratory of High Performance Ceramics and Superfine Microstructures, Shanghai Institute of Ceramics, Chinese Academy of Sciences, Shanghai 200050, China*

ABSTRACT

Relaxor ferroelectrics with extraordinary properties are useful for developing various kinds of electronic devices. An unique relaxor ferroelectric series is the perovskite solid solution between $Pb(Zn_{1/3}Nb_{2/3})O_3$ and $BaTiO_3$ [(1−*x*)PZN-*x*BT], because of its uncommon phase transition behavior. The temperature dependent permittivity, dielectric relaxation, thermal expansion, local polar structure and hysteresis loop were investigated in the present work. "U" shape curves were observed of the T_m, ε_m, P, E_c and P_r in BT content range from 0.1 to 0.9. A polarization mismatched model was proposed to illustrate the underlying mechanism.

1. Introduction

With the development of power electronics, increasing interest has been aroused about dielectric materials for energy-storage capacitors due to their high-energy storage density, low loss and good temperature stability [1-3]. In order to design proper dielectrics for energy storage application, three requirements must be satisfied at the same time: large saturated polarization (P_s), small remnant polarization (P_r), and high electric breakdown field strength [4]. Relaxor ferroelectrics exhibit high P_s, low P_r and slim hysteresis loop, which make them meet the requirements for energy storage application. Particularly, the relaxor ferroelectrics can exhibit good temperature stability due to their diffuse phase transition (DPT) behavior around the dielectric peak. Compositional disorder, for example, the disorder in the arrangement of different ions on the one unit site is a common feature of relaxors ferroelectircs [5]. Some traditional relaxor ferroelectrics with $Pb(B'B'')O_3$perovskite structure, such as $Pb(Mg_{1/3}Nb_{2/3})O_3$ (PMN) and $Pb(Zn_{1/3}Nb_{2/3})O_3$ (PZN), where the B-site are occupied by two kinds of cations, have been extensively investigated owing to their unique relaxor behavior. However, This kind of canonical relaxor ferroelectrics are not suitable for energy storage application, owing to their poor temperature stability [6-8]. In order to meet the needs of practical application, more attention has been paid on developing new material systems.

Recently, Some solid solution of Bi-based perovskite compound doped with $BaTiO_3$ (BT) have aroused much interest due to their good temperature stability, such as $BaTiO_3$-$BiScO_3$ (BT-BS) [9-11], $BaTiO_3$-$Bi(Mg_{1/2}Ti_{1/2})O_3$ (BT-BMT), [12-13] and $BaTiO_3$-$Bi(Mg_{1/2}Nb_{1/2})O_3$ (BT-BMN) [14]. In many cases, as the Bi-based perovskite content increases, the crystal structure changes from tetragonal to pseudocubic phase. The phase transition is also accompanied by a change in dielectric properties from normal ferroelectric to relaxor-like behavior [14-15]. PZN is a typical relaxor ferroelectric with rhombohedral

perovskite structure at room temperature. It has a high dielectric constant (ε_{max}≈22000 in single crystal) around the Curie temperature (T_C), and shows obvious DPT behavior [19-20]. Single phase of perovskite structure can be synthesized in PZN-based solid solutions such as $Pb(Zn_{1/3}Nb_{2/3})O_3$-$BaTiO_3$ (PZN-BT) [21], $Pb(Zn_{1/3}Nb_{2/3})O_3$-$SrTiO_3$ (PZN-ST) [22], and $Pb(Zn_{1/3}Nb_{2/3})O_3$-$PbTiO_3$ (PZN-PT) [23], where BT, PT and ST are usually used to stabilize the phase structure. Among these additives, BT is the most effective to suppress the formation of the pyrochlore phase and stabilize phase structure. All the PZN-PT compositions shows slight peak shift (ΔT_C=2 °Cat most) and weak DPT behavior [24], while all the compositions shows strong DPT behavior in the PZN-BT system. This obvious contrast has also been observed in PMN-PT and PMN-BT system. Wang *et al*. reported that BZN-rich paraelectric phase might be present in PZN-BT ceramics, making the system even more complicated [25,26]. Moreover, Li *et al*. reported that DPT behavior might be caused by the presence of paraelectric phase $Ba(Mgn_{1/3}Nb_{2/3})O_3$ in PMN-BT ceramics [27]. However, there is lacking of direct evidence for presence of BZN in above systems.

In a previous work, solid solution of the (1−*x*)PZN-*x*BT were studied byArvind *et al.*[21]. However, their investigations of the PZN-BT solid solutions pay more attention to demonstrate that $BaTiO_3$ is an excellent additive for stabilizing perovskite structure in PZN. In this work, PZN-BT is considered as a typical mismatch lead-based relaxor ferroelectrics. We focus on the effects of the BT content on microstructure, dielectrics properties phase transition and polarization behaviors of the PZN-BT system.

2. Experimental procedure

The compositions selected for this study were (1-*x*)$Pb(Zn_{1/3}Nb_{2/3})O_3$-*x*$BaTiO_3$(*x* = 0.1~0.9). The reagents of PbO (99.9%), ZnO (99.9%), Nb_2O_5 (99.9%), TiO_2 (99.9%) and

$BaCO_3$ (99.9%) were used as starting raw materials (Sinopharm Chemical Reagent Co. Ltd, Shanghai, China). The ceramics were prepared by means of a two-step columbite reaction method. First, ZnO and Nb_2O_5 mixed in stoichiometric ratio were ball-milled for 12 h. After drying, the mixtures were calcined at 1000 ^oC for 6 h. Then the precursor was mixed with PbO, TiO_2 and $BaCO_3$ in stoichiometric ratio and milled for 12h. After drying, the powders were pre-sintered at 900 ^oC for 2 h in a sealed Al_2O_3 crucible. The pre-sintered powders were ball milled and dried again. The dried powders were well mixed with a 5 wt.% PVA binder, pressed into 12 mm in diameter and 1mm in thickness pellets under a pressure of 150 MPa. The binder was burnt out at 600 °C for 2h in air. Finally, the samples were sintered at temperature range from 1190 °C to 1350 ^oC in a sealed Al_2O_3 crucible in case PbO evaporation from the pellets.

Phase structure of the ceramics samples was examined by X-ray diffractometer (XRD , Rigaku D/Max-2400 , Tokyo, Japan) using CuKα radiation (λ = 0.15406 nm) operating at 40 kV and 100 mA. The microstructure of the ceramics samples was observed by using scanning electron microscopy (SEM, FEI Quanta 250 FEG, Hillsboro, OR). The dielectric temperature spectra were measured by a LCR meter (Agilent HP4284A, Santa Clara, CA, USA) with a frequency range from 100 Hz to 100 kHz. Ferroelectric polarization-electric field (*P*-*E*) hysteresis loops were measured at 1 Hz using a ferroelectric test system (TF Analyzer 2000E, aixACCT, Aachen, Germany). The linear thermal expansion has been measured in the temperature range 100-650 K using the induction pushrod dilatometer Netzsch DIL-402C calibrated with a silica glass as a standard.

3. Results and Discussion

XRD patterns of the (1-*x*)PZN-*x*BT (*x*=0.1~0.8) with a scanning angle from 20^o to 70^o

are shown in Fig. 1(a). The XRD results suggest a pure perovskite structure without any detectable pyrochlore phase. In addition, no distinct peak splitting for the (200) peak, which corresponds to a tetragonal symmetry, was detected in Fig. 1(b). Therefore, the phase structure could be pseudocubic perovskite structure. With the increase of BT content, the diffraction peaks gradually move toward higher degree [Fig. 1(b)]. This phenomenon indicates that the cell volumes decrease with the increase of BT content. Ba^{2+}(1.61 Å) is larger than Pb^{2+}(1.49 Å), whereas Ti^{4+}(0.605 Å) is smaller than Zn^{2+} (0.74 Å) and Nb^{5+}(0.64 Å) which occupy B-site. The equivalent ionic radii of Zn^{2+} and Nb^{5+} can be calculated by □ = 1/3 □=0.673 Å. The crystal cell radiusdecreases with the increase of BT content, indicating that in the PZN-BT perovskite structure, the B-O_6 octahedra dominates the unit cell volume.

Fig. 2 reveals the SEM micrographs from the thermally etched surface of PZN-BT ceramics. It is found that the samples are of full dense and have clear grain boundaries. The grain size is not quite uniform. With the increase of BT content, the grain size decreases obviously.

Fig. 3 shows the dielectric constant and loss tangent measured at 0.1, 1, 10, 50 and 100 kHz as a function of temperature. The PZN-BT ceramics exhibit obvious DPTs. Meanwhile, the dielectric dispersion of the dielectric permittivity and dielectric loss can be seen clearly which demonstrates typical relaxor behavior. The temperature dependence of dielectric constant (at 1 kHz) for a range of compositions is shown in Fig. 4(a). For $0.5 \leq x \leq 0.7$, the dielectric peaks become broader. Correspondingly, the maximum permittivity (ε_{max}) values and T_{max}, at which the maximum permittivity was observed, also become smaller.

Fig. 4(b) presents the T_{max} and ε_{max}as a function of BT content in the (1-x)PZN-xBT system. The T_{max} first decreased with x value from 140 °C at $x = 0$ for pure PZN to −117 °C at

x = 0.7, and then increased with x from −117 °C at x = 0.7 to 120 °C at x = 1.0 for pure BT. The change trend of T_{max} with composition is in the form of a "U" curve. According to Xiong *et al.*'s assumptions [29], in the PZN-BT system, the low level of PZN results in little interaction of Pb^{2+}, Zn^{2+}, and Nb^{5+} ions, is similar to PbO, ZnO and Nb_2O_5 oxide-doped BT compounds, resulting in the depression of T_m. However, the interaction of these ions was enhanced when the PZN reached a certain level ($x \geq 0.8$). Moreover, the variation of the ε_{max} is in accord with T_{max}.

The emergence of the relaxor behavior caused by the addition of PZN in the BT ceramics is in accord with *Setteret et al.*' s [30] and *Bokov et al.*' s [5] assumptions. According to their assumptions, the large difference in the valence between B′ and B″ ions and small size of A-site cation would enhance the elastic drive toward ordering on the B-site in $A(B'B'')O_3$ system, and the DPT would be sharpened by increase in the B-cation ordering. In this work, it can be seen that Pb^{2+} ion has smaller radius than Ba^{2+} ion on the A-site, whereas both Zn^{2+} and Nb^{5+} ions have smaller radius than Ti^{4+} ion on the B-site, which would cause relaxor behavior in PZN-BT system. For relaxor ferroelectrics, the relaxor properties can be analyzed by a modified Curie-Weiss law [30-31], which can be written as:

$$\frac{1}{\square} - \frac{1}{\square_{\square\square\square}} = \frac{\square\square - \square_{\square}\square^{\square}}{\square}, \qquad (1)$$

where ε_{max} is the maximum value of the dielectric permittivity, T_m is the temperature for ε_{max},C is the Curie-like constant, and γ is the degree of diffuseness. For γ=1, the formula (1) is equivalent to Curie-Weiss law, applying to the case of normal ferroelectrics. The fitting to Eq. (1) are shown in Fig. 5. The values of γ for (1−x)PZN-xBT (x = 0.1~0.8) by fitting are shown in Table 1, indicating that these compositions might have similar relaxor behavior. However, the Eq. (1) cannot describe variation law of relaxor behavior of all the compositions accurately. Therefore, the new glass model is introduced to characterize relaxor behavior

[32],

$$\omega = \omega_0 \exp\left(-\frac{E_0}{k_B T_m}\right) \quad (2)$$

The Eq. (2) characterizes the relation between the frequency (ω) and the temperature (T_m) at the dielectric peak of the relaxor ferroelectrics. The value of parameter p can be used to describe the dielectric relaxation strength (DRS) and relation among normal ferroelectrics, relaxor ferroelectrics, the Debye medium and glass. For relaxor ferroelectrics, the value of p is larger than 1, and increases with decreasing of the DRS. Logarithm of frequency [$\ln\omega$] as a function of reciprocal of temperature [$1/T$] and the fitting to the Eq. (2) are shown in Figure 6. The values of P for (1−x)PZN-xBT (x = 0.1~0.8) by fitting are summarized in Table 2. It is clear that the addition of PZN caused a shift toward relaxor ferroelectrics. This phenomenon is in accord with Xiong *et al.*'s assumptions, and has also been noted in other relaxor system [14,16,33,].

The ΔT_m has been introduced for further comparison of relaxation behavior quantitatively. The ΔT_m, which is used to characterize the degree of frequency dispersion in the frequency range from 100 Hz to 100 kHz, is defined as follows: [34]

$$\Delta T_m = T_{m(100\ \mathrm{kHz})} - T_{m(100\ \mathrm{Hz})}, \quad (3)$$

where $T_{m\ (100\ \mathrm{kHz})}$ and $T_{m\ (100\ \mathrm{Hz})}$ are the temperature of dielectric peak measured at 100 kHz and 100 Hz, respectively. The values of P and ΔT_m for PZN-BT system are showed in Fig. 7(a) and (b). The change trend of ΔT_m shows the positive relation with the trend of P (except for x = 0.3 sample). It is reasonable to believe that the new glass model can characterize relaxor behavior for PZN-BT system properly. In general, the disorder in the arrangement of different ions on the crystallographically equivalent sites is the common feature of relaxor ferroelectrics. In this work, the substitution of the Ba^{2+} by Pb^{2+} and Ti^{4+} by Zn^{2+} and Nb^{5+}

enhance the positional disorder in A- and B-site ions of ABO_3 perovskite, consequently, leading to the increasing relaxor behavior.

Temperature dependencies of thermal expansion coefficient (α) and strain ($\Delta L/L$), for samples with x = 0.5~0.7, are presented in Fig. 8(a) and (b) (solid line). Measurements were performed in dynamical mode with heating and cooling rate 2-3 K/min in a flow of dry helium (O_2 concentration is about 0.05% of volume).The sample loading was 30 cN. There is no clear anomaly characteristic for phase transition was observed for all the samples in temperature range of measurement.In general temperature-independent α corresponding to linear thermal expansion or weakly temperature-dependent α are expectedin pure paraelectric state [35-37]. The Burns temperature (T_d) is identified as the temperature, where remarkable deviation from such regular behavior starts in direction of low temperature. To separate lattice (regular) and anomalous contributions to the thermal expansion in wide temperature range, the relation [38]

□ □□ □ = □□ + □□ □□□,□ □□, (4)

was used, where $C_D(T,\theta_D)$ is Debye model heat capacity, θ_D is Debye temperature.

□ □□ □ = 9□ (5)

Fig. 8(a-b) (dot line) indicate that such fitting is suitable for our case with $\theta_D \approx$ 461, 431 and 522 K for x = 0.5, 0.6 and 0.7 respectively. Temperature dependency of anomalous $\Delta\alpha$ and $\Delta(\Delta L/L)$, for samples with x = 0.5~0.7, are presented in Fig. 9(a) and (b). The depletion point—T_d can be estimated from temperature dependency of anomalous strain, and T_m can be defined from anomalous $\Delta\alpha(T)$. For all the compounds, $T_d \approx$ 500 ±50 K. $T_m \approx$ 270 K for x = 0.5, and $T_m \approx$ 220 K for x = 0.6. Samples (x = 0.5~0.7) possess similar T_d value, even though there are differences in their compositions. At the temperature blow T_d, temperature

dependence of $\Delta L/L$ deviates from linear behavior (characteristic of high temperature), which is considered as the onset of polar nanoregions (PNRs). The deviation of strain from classical theory comes from the local electrostriction effect of PNRs.

The ferroelectric *P-E* hysteresis loops measured at room temperature and 1 Hz for (1−*x*)PZN-*x*BT are shown in Fig. 10(a). Slim hysteresis loops, which demonstrate typical relaxor behavior [39], are observed in these ceramics. For x = 0.1, the *P-E* hysteresis loop shows a tendency towards saturation at such a low electric field (≈ 20 kV/cm), which is similar to that of normal ferroelectrics. Fig. 10(b) shows the P_r and E_c summarized at room temperature at 1 Hz as a function of the BT content. With the increase of the BT content, the P_r and the E_c are also in the form of "U" curve. This phenomenon may be related to the variation of ΔT_m,which is used to characterize the degree of frequency dispersion, as shown in Fig. 7(b). It is reasonable to infer that the variation of hysteresis behavior derive from the disorder in the structure due to the substitution of the Ba^{2+} by Pb^{2+} and Ti^{4+} by Zn^{2+} and Nb^{5+}.

In general, PZN-BT shows interesting dielectric relaxation and phase transition behaviors, where, the T_{max}, P_r, and E_c vary in the form of "U" shape curve with the composition variation. To our understanding, the ferroelectricity of PZN comes mainly from the ordering of electronic and ionic coupling between A site and O site (A-O coupling), while that of BT mainly from the B-O coupling[40]. As BT is introduced to PZN, the A-O ordering may be disrupted by barium occupying A site, leading to decreased T_m. On the other hand, the B-O ordering will also be affected by zinc and niobium occupying B site in case of PZN doped to BT. In the intermediate compositions, neither A-O ordering nor B-O ordering can be established. In other words, the polarization mismatch happens. This picture is almost the same with the previous concept "nano phase separation" proposed in the same material system by Wang[25-26]. The main difference here is we emphasis the fluctuation of polarization and ferroelectric order, rather than chemical composition.

The polarization mismatch cancels long range ferroelectric order by cross occupying in both A-site and B-sites. Microscopically, local regions at nanometer scale fluctuate in composition and consequently, in polarization. This structural feature leads to peculiar characteristics, such as low T_m, broadened dielectric peak and slim hysteresis loop. Similar phenomena can also be observed in bismuth based solid solution systems, including BMT-BT[12-13], BMN-BT[14] and BS-BT[9-11].The common features of these material systems may arise from polarization mismatch.

A sharp contrast was observed for the above materials systems if replace BT with PT, where normal ferroelectric such as PMN-PT and PZN-PT, BF-PT, BS-PT appear. [23-24,41] No "U"shape curve can be seen, because PT has A-O coupling and no polarization mismatch happens. This proof supports the polarization mismatch explanation.

4. Conclusions

In this work,the composition dependence of the properties of (1-*x*)PZN-*x*BT solid solutions (x = 0.1~0.8) were studied. Normal ferroelectric BT doped with relaxor ferroelectric PZN produces a new relaxor ferroelectric (1-*x*)PZN-*x*BT with unique dielectric behavior. The T_{max}, P_r, and E_c are in the form of "U" shape curve.A polarization mismatch model was proposed to illustrate the underlying mechanism

Acknowledgments

This work is supported by the Natural Science Basis Research Plan in Shaanxi Province of China (Grant No. 2015JM5199), the Fundamental Research Funds for the Central Universities, the National Basic Research Program of China (973 Program) (Grant No. 2015CB654602), the International Science & Technology Cooperation Program of China (Grant Nos. 2013DFR50470 and 2015DFA51100), the 111 Project under Grant No. B14040.

Figure captions

Fig. 1. (a) XRD patterns of (1−*x*)PZN-*x*BT (*x*=0.1~0.8) ceramic samples with a scanning angle from 20º to 70º. (b) Enlarged XRD patterns from 45.0º to 46.0º of (1−*x*)PZN-*x*BT ceramics.

Fig. 2. SEM images of thermally etched surfaces of the (1−*x*)PZN-*x*BT ceramics sample with *x*= 0.1~0.8, corresponding to (a) ~ (h). Thermal etching was performed at 100 °C below the sintering temperature of PZN-BT ceramics for 30 min.

Fig. 3. The dielectric constant and loss tangent as a function of temperature measured at 0.1, 1, 10, 50 and 100 kHzfor (1−*x*)PZN-*x*BT ceramic samples with *x*=0.1~0.8, corresponding to (a) ~ (h). The heating rate is 3ºC/min.

Fig. 4. Variation of dielectric constant (1 kHz) with temperature in the (a) for (1-*x*)PZN-*x*BT compositons, *x*=0.2 ~ 0.8. T_{max} and ε_{max} vs composition in the (b) for (1-*x*)PZN-*x*BT, *x* = 0.1~0.8, at 1 kHz, where the datafor pure PZN and BT are from published results. [21,28]

Fig. 5. (Dot lines) Processed dielectric constant [$\ln(C(1/\varepsilon-1/\varepsilon_m))$] as a function of logarithm of temperature [$\ln(T-T_m)$] at 1 kHz for (1-*x*)PZN-*x*BT, where *x*= 0.1~0.8, correspondingto (a) ~ (h). Solid lines are the fittings to the Eq. (1), for (1-*x*)PZN-*x*BT : *x*= 0.1~0.8, corresponding to (a) ~ (h).

Fig. 6. (Scatter dots) Logarithm of frequency[$\ln\omega$] as a function of reciprocal of temperature [1/T] for (1-*x*)PZN-*x*BT, where *x*= 0.1~0.8, corresponding to (a) ~ (h).

Solid lines are the fittings to the Eq. (2), for (1-*x*)PZN-*x*BTceramic samples with *x*=0.1~0.8, corresponding to (a) ~ (h).

Fig. 7. Variation of P in the (a) and ΔT_m,where $\Delta T_m = \Delta T_{m(100\ kHz)} - \Delta T_{m(100\ Hz)}$, in the (b) vs composition in PZN-BT system.

Fig. 8. Temperature dependence of thermal expansion coefficient α(a) and strain$\Delta L/L$ (b) for (1-x)PZN-xBT ceramics, ($0.5 \leq x \leq 0.7$) (solid linesareexperimental data and dot linesareapproximated by relation (4))

Fig. 9. Temperture dependence of anomalous thermal expansion coefficient$\Delta\alpha$in the(a) and strain$\Delta L/L$ in the (b) for (1-x)PZN-xBT ceramics, ($0.5 \leq x \leq 0.7$)

Fig. 10. (a)P-E hysteresis loops of PZN-BT ceramics measured at ambient temperature with a triangular wave form at 1HZ. (b) the remanent polarization (P_r) and coercive field (E_c) summarized at room temperature and 1Hz as a function of BT content for (1-x)PZN-xBT ceramics, ($0.2 \leq x \leq 0.8$)

Table 1. The value of γ for (1−x)PZN-xBT ceramic samples.

x	0.1	0.2	0.3	0.4	0.5	0.6	0.7	0.8
γ	1.81	1.64	1.89	1.65	1.79	1.82	1.71	1.83

Table 2. The value of p for (1−x)PZN-xBT ceramic samples.

x	0.1	0.2	0.3	0.4	0.5	0.6	0.7	0.8
p	9.77	5.66	8.20	2.20	2.26	1.81	2.43	4.03

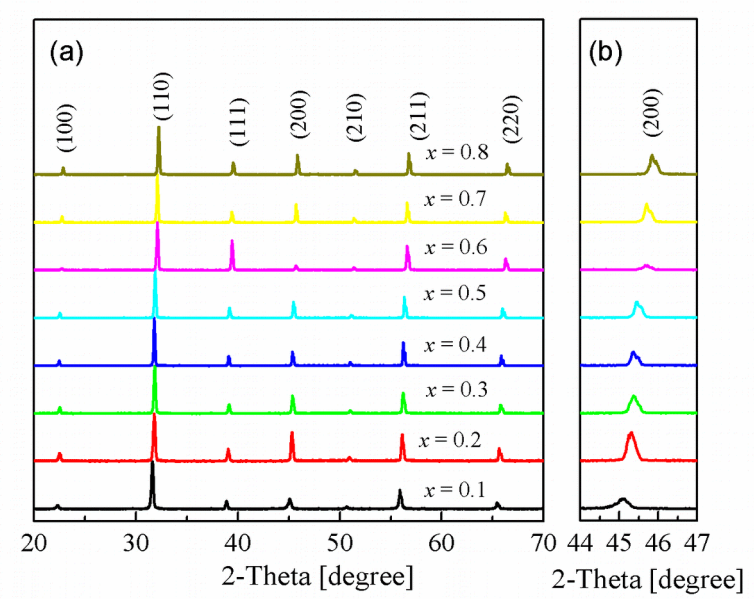

Fig. 1. Fig. 1. (a) XRD patterns of (1−*x*)PZN-*x*BT (*x*=0.1~0.8) ceramic samples with a scanning angle from 20º to 70º. (b) Enlarged XRD patterns from 45.0º to 46.0º of (1−*x*)PZN-*x*BT ceramics.

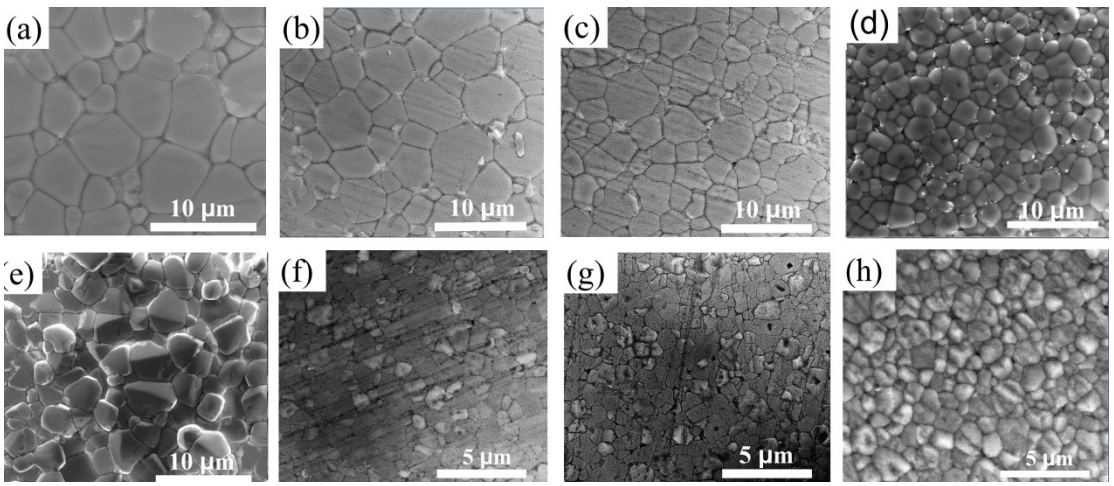

Fig. 2. Fig. 2. SEM images of thermally etched surfaces of the (1−*x*)PZN-*x*BT ceramics sample with *x*= 0.1~0.8, corresponding to (a) ~ (h). Thermal etching was performed at 100 °C below the sintering temperature of PZN-BT

ceramics for 30 min.

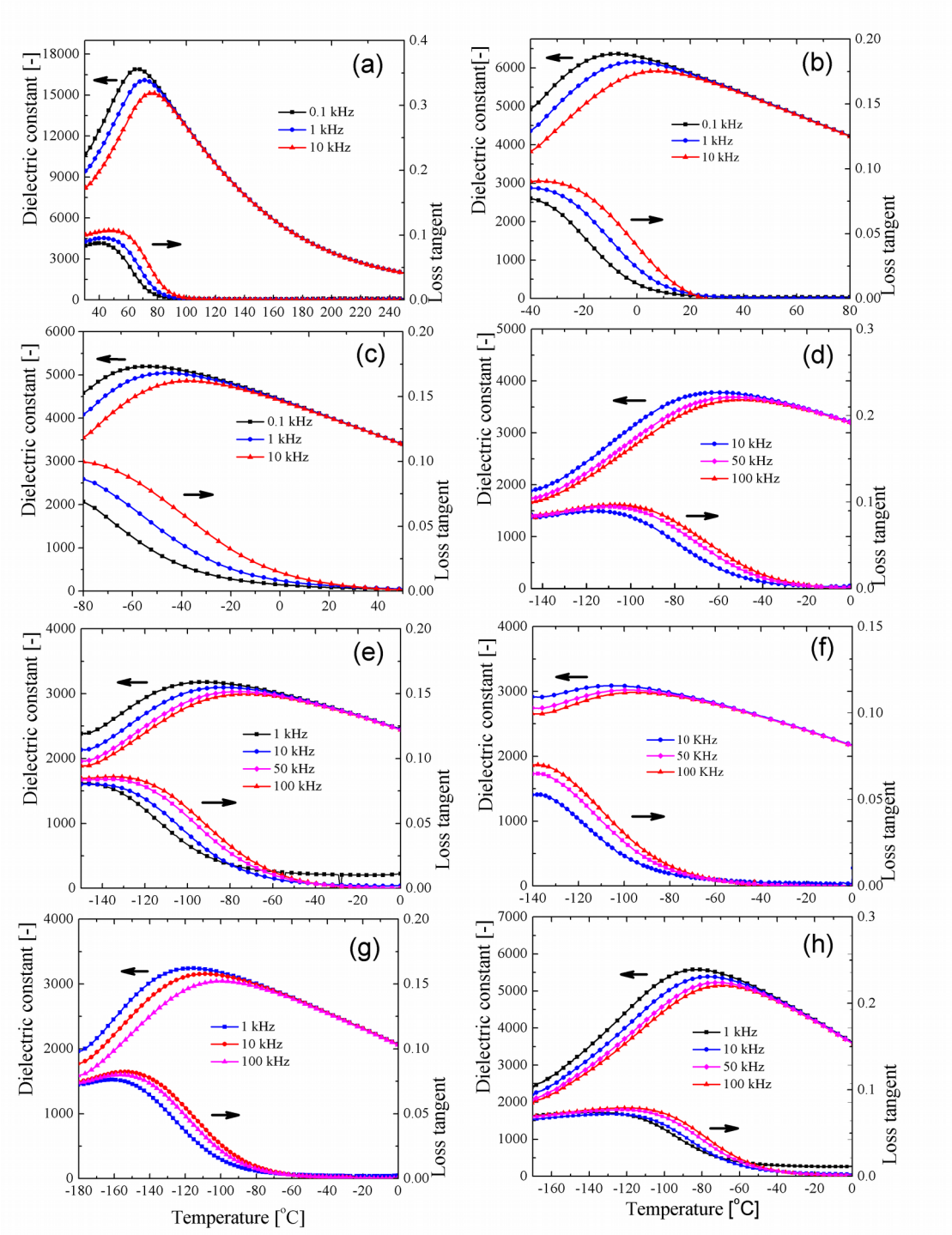

Fig. 3. The dielectric constant and loss tangent as a function of temperature measured at 0.1, 1, 10, 50 and 100 kHz for (1−*x*)PZN-*x*BT ceramic samples with *x*=0.1~0.8, corresponding to (a) ~ (h). The heating rate is 3°C/min.

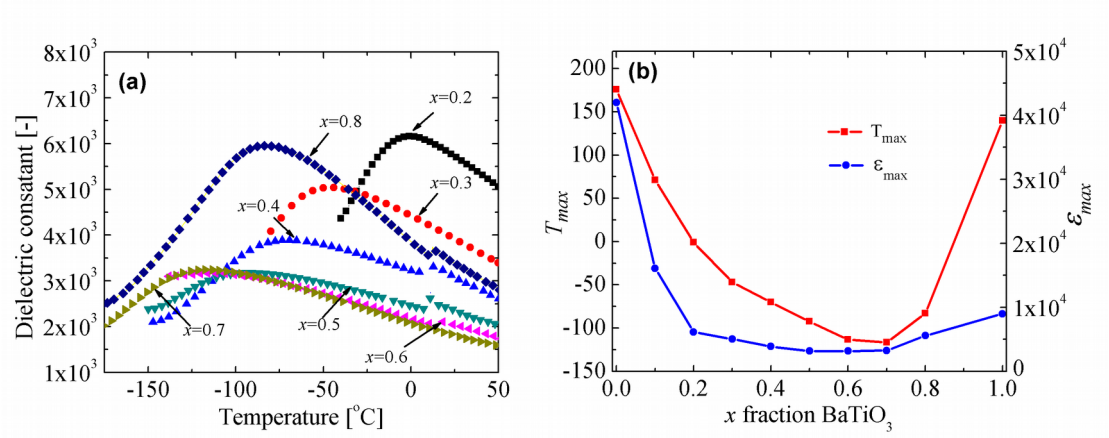

Fig. 4. Variation of dielectric constant (1 kHz) with temperature in the (a) for (1-*x*)PZN-*x*BT compositons, *x*=0.2 ~ 0.8. ₸*T*max and ε_{max} vs composition in the (b) for (1-*x*)PZN-*x*BT, *x* = 0.1~0.8, at 1 kHz, where the datafor pure PZN and BT are from published results. [21,28]

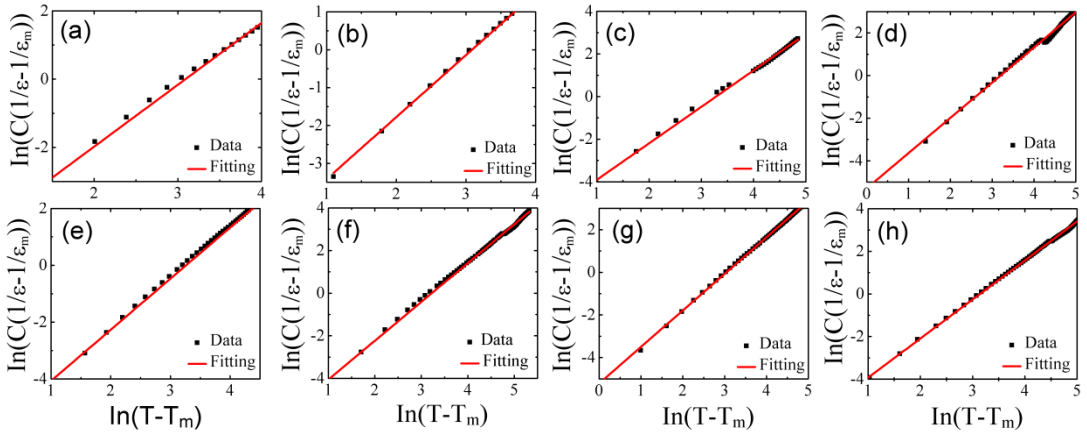

Fig. 5. (Dot lines) Processed dielectric constant [$\ln(C(1/\varepsilon-1/\varepsilon_m))$] as a function of logarithm of temperature [$\ln(T-T_m)$] at 1 kHz for (1-*x*)PZN-*x*BT, where *x*= 0.1~0.8, correspondingto (a) ~ (h). Solid lines are the fittings to the Eq. (1), for (1-*x*)PZN-

*x*BT : *x*= 0.1~0.8, corresponding to (a) ~ (h).

Table 1. The value ofγfor(1-*x*)PZN-xBT

x	0.1	0.2	0.3	0.4	0.5	0.6	0.7	0.8
γ	1.81	1.64	1.89	1.65	1.79	1.82	1.71	1.83

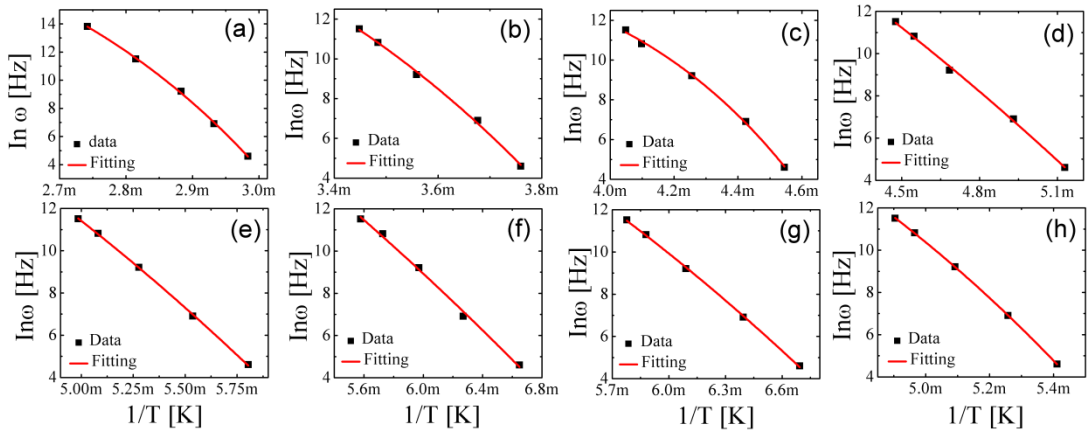

Fig. 6. (Scatter dots) Logarithm of frequency [lnω] as a function of reciprocal of temperature [1/T] for (1-*x*)PZN-*x*BT, where *x*= 0.1~0.8, corresponding to (a) ~ (h). Solid lines are the fittings to the Eq. (2), for (1-*x*)PZN-*x*BTceramic samples with *x*=0.1~0.8, corresponding to (a) ~ (h).

Table 2. The value of P for (1-x)PZN-xBT

x	0.1	0.2	0.3	0.4	0.5	0.6	0.7	0.8
P	9.77	5.66	8.20	2.20	2.26	1.81	2.43	4.03

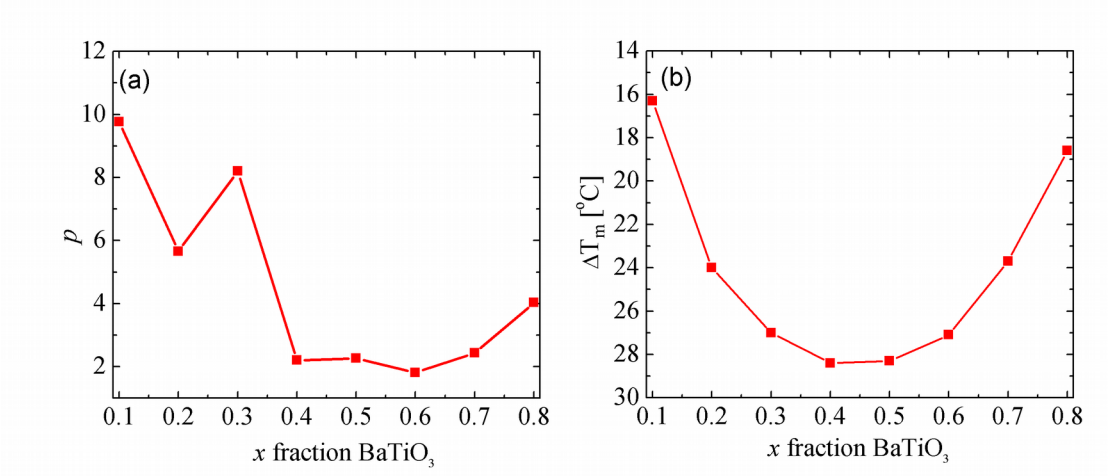

Fig. 7. Variation of P in the (a) and ΔT_m,where $\Delta T_m = \Delta T_{m(100\ kHz)} - \Delta T_{m(100\ Hz)}$,in the (b) vs composition in PZN-BT system.

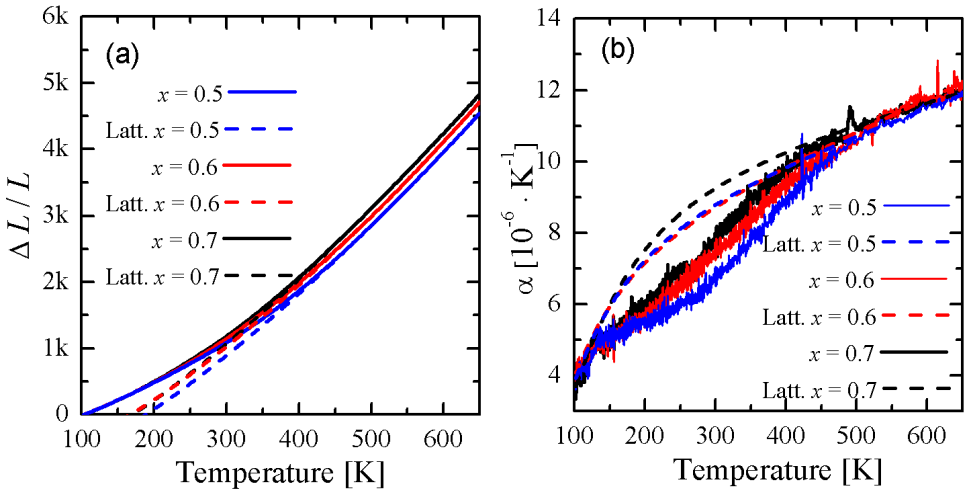

Fig. 8. Temperature dependence of thermal expansion coefficient α(a) and strain$\Delta L/L$ (b) for (1-x)PZN-xBT ceramics, ($0.5 \leq x \leq 0.7$) (solid linesareexperimental data and

dot linesare approximated by relation (4))

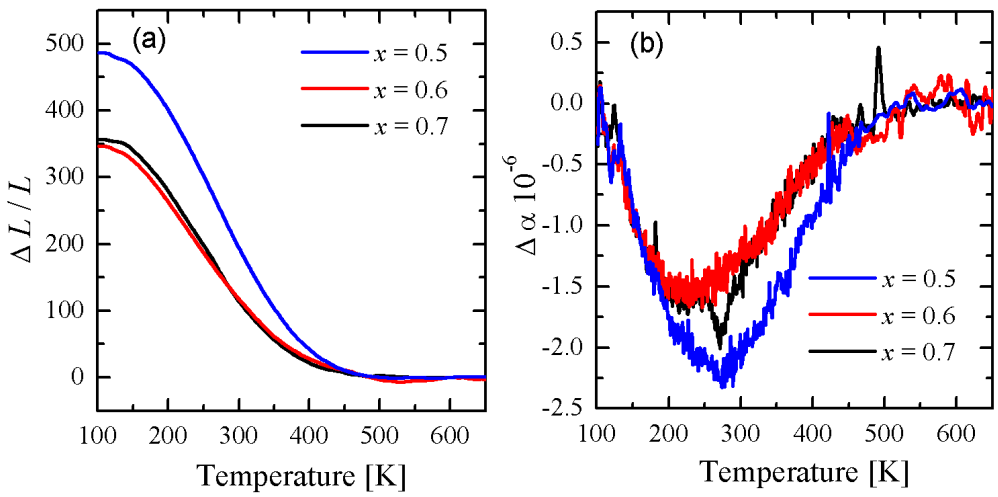

Fig. 9. Temperture dependence of anomalous thermal expansion coefficient$\Delta\alpha$in the(a) and strain$\Delta L/L$ in the (b) for (1-x)PZN-xBT ceramics, ($0.5 \leq x \leq 0.7$)

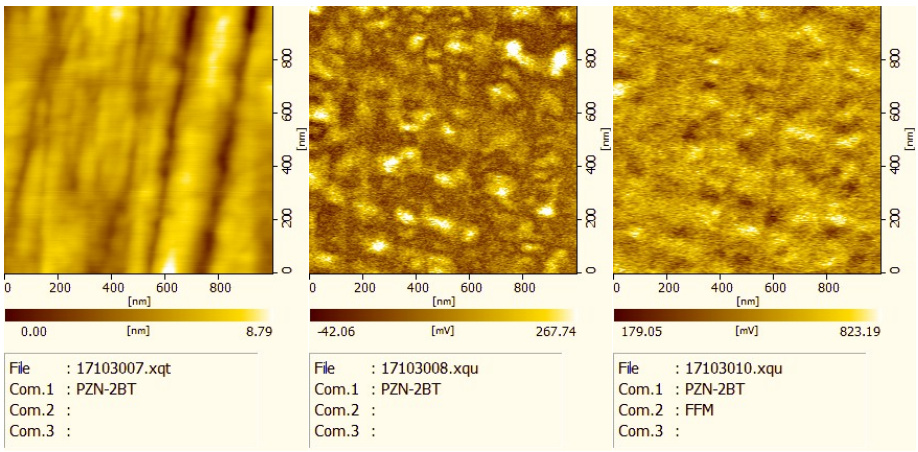

....

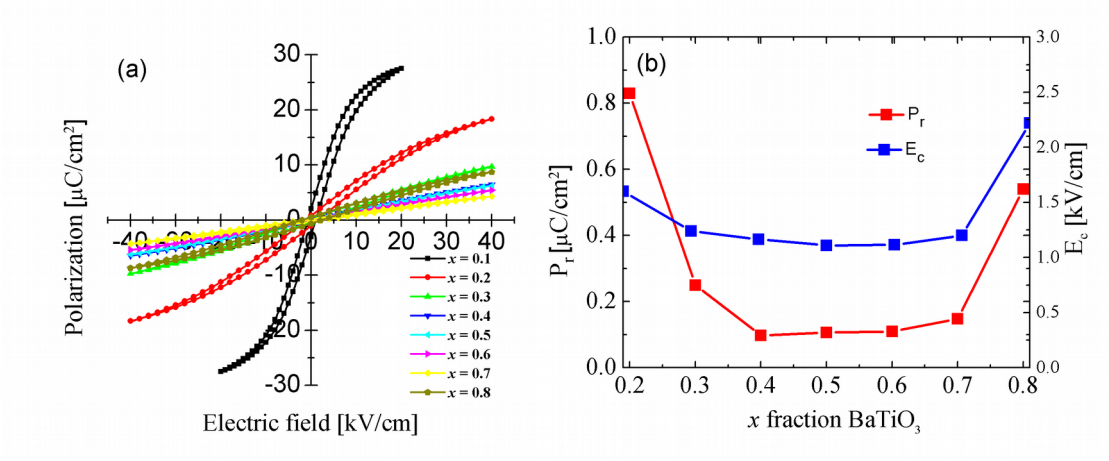

Fig. 10. (a)*P-E* hysteresis loops of PZN-BT ceramics measured at ambient temperature with a triangular wave form at 1HZ. (b) the remanent polarization (P_r) and coercive field (E_c) summarized at room temperature and 1Hz as a function of BT content for (1-x)PZN-xBT ceramics, ($0.2 \leq x \leq 0.8$)